UCRL--93858

DE86 005620

RADIATING SHOCKS AND CONDENSATIONS IN FLARES *

George H. Fisher

Institute of Geophysics and Planetary Physics
Mail Code L-413
Lawrence Livermore National Laboratory
Livermore, California 94550
U.S.A.

* Work performed under the auspices of the U.S. Department of Energy by the Lawrence Livermore National Laboratory under contract number W-7405-ENG-48.

ABSTRACT

Rapid energy release (by either "thick target" (beam) or "thermal" models of heating) in solar flare loop models usually leads to "chromospheric evaporation", the process of heating cool chromospheric material to coronal temperatures, and the resulting increase in hot soft X-ray emitting plasma. The evaporated plasma flows up into the coronal portion of the loop because of the increased pressure in the evaporated region. However, the pressure increase also leads to a number of interesting phenomena in the flare chromosphere, which will be the subject of this paper. The sudden pressure increase in the evaporated plasma initiates a downward moving "chromospheric condensation", an overdense region which gradually decelerates as it accretes material and propagates into the gravitationally stratified chromosphere. Solutions to an equation of motion for this condensation shows that its motion decays after about one minute of propagation into the chromosphere. When the front of this downflowing region is supersonic relative to the atmosphere ahead of it, a radiating shock will form. If the downflow is rapid enough, the shock strength should be sufficient to excite UV radiation normally associated with the transition region, and furthermore, the radiating shock will be brighter than the transition region. These results lead to a number of observationally testable relationships between the optical and ultraviolet spectra from the condensation and radiating shock.

1. DESCRIPTION OF THICK TARGET AND THERMAL MODEL FLARE SIMULATIONS

The results of flare heating in a thick target simulation (Fisher, Canfield, and McClymont 1985a, henceforth FCMa) are shown in Figure 1. A preflare loop model (An et al, 1983) is subjected to bombardment by an

intense flux of energetic electrons. Shortly after the onset of electron heating at t=0 [s], the topmost portion of the chromosphere heats up very rapidly (on a time scale of about 1 second) to coronal temperatures. This seems to happen more or less at constant density, resulting in a large overpressure in this region. This overpressure quickly begins to drive upward motion of the heated material at speeds in excess of several hundred [km s^{-1}]. At the same time, the overpressure also begins to drive downflows into into the remaining portion of the chromosphere, but at speeds generally less than 100 [km s^{-1}]. Interestingly, this downflowing region is both much denser and much cooler than the chromospheric material ahead of it. The effects of heating by nonthermal electrons below this downward moving "chromospheric condensation" seem mainly to be the heating of the chromosphere sufficiently to ionize it, and to maintain a quasi-steady balance between heating by the nonthermal electrons and the dominant radiative loss mechanism, which in this case is optically thin metal losses.

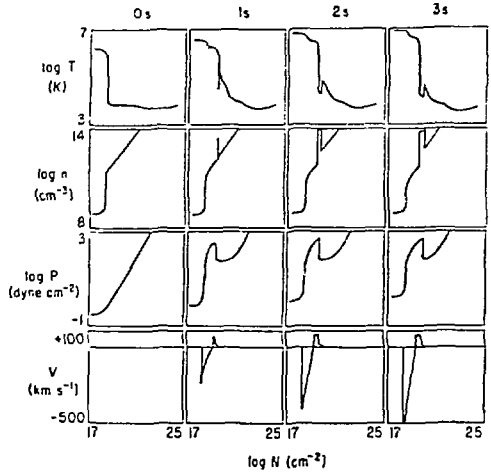

Figure 1. Evolution of temperature, number density, pressure, and velocity in the loop atmosphere for a thick target energy flux of 10^{11} [erg cm^{-2} s^{-1}]. The column depth N is measured from the loop apex. Note velocities away from the loop apex (i.e. downward) are considered positive

In the thermal model of flare heating, illustrated in Fig. (2), the evolution of the same initial loop atmosphere is somewhat different. After heating commences at t=0 [s], the upper portion of the corona corresponding to the energy deposition region rapidly achieves a temperature of roughly $3x10^7$ [K], after which the additional flare heating goes into driving a saturated conduction front into the remaining portion of the ambient corona. It takes nearly 25 [s] for the conduction front to traverse the 30000 [km] coronal portion of the loop before finally reaching the chromosphere. During this time, the coronal plasma is actually moving downward. When the front hits the top of the

chromosphere, it begins to rapidly heat the dense material to temperatures of roughly 10^7 [K], resulting in a local overpressure, although not as great as that for thick target explosive evaporation. This overpressure then drives upward motion of the heated material, reversing the earlier downward motion of coronal plasma. The upflow speeds, however, are not as great as in the thick target case, being just over 100 [km s^{-1}]. The overpressure also drives downflow into the chromosphere, as with the thick target case, but the temperatures involved are much lower, since there is not any direct heating source in the chromosphere. The amplitude of the downflow speed is also less, a result of the reduced overpressure. The dominant radiative loss mechanisms in the chromosphere for thermal model heating seem to be optically thick emission from hydrogen and singly ionized calcium and magnesium.

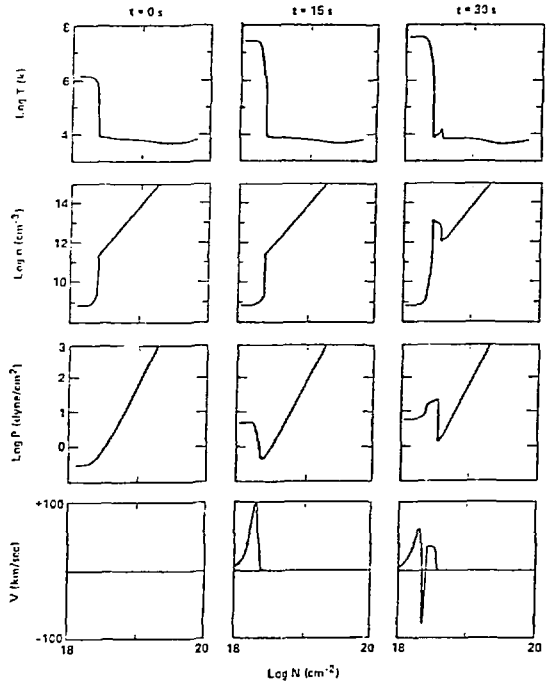

Figure 2. Evolution of temperature, number density, pressure, and velocity in the loop atmosphere for thermal model heating with an energy input rate of 10^9 [erg cm^{-2} s^{-1}]. The column depth N is measured from the loop apex. Note velocities away from the loop apex (i.e. downward) are considered positive

2. FORMATION AND EVOLUTION OF CHROMOSPHERIC CONDENSATIONS

One of the most striking features seen in Figures 1 and 2 showing the response of the loop atmosphere to impulsive phase flare heating is the formation in the chromosphere of downward moving, overdense

regions. Furthermore, in the thick target case (Fig. 1) the downflowing dense plasma is also significantly cooler than its surroundings. These "chromospheric condensations" form shortly after the onset of chromospheric evaporation, and are in fact driven by the evaporation process. In the case of thick target evaporation (Fig. 1) the pressure in the evaporated region exceeds the overlying coronal pressure as well as the pressure in the chromosphere. This results in driving both upward motion (evaporation) and the downward moving chromospheric condensation. The hydrodynamic response for the thermal model (Fig. 2) is similar: The downward moving conduction front hits the top of the chromosphere, suddenly creating a local pressure maximum at that point. Again, this drives both upflows (evaporation) and downflows (the chromospheric condensation), as the conduction front propagates into the chromosphere.

The structure of the chromospheric condensation is as follows: If the condensation's velocity is supersonic relative to the material ahead of it, the leading edge of the condensation consists of a hydrodynamic shock, of order one proton-proton mean free path thick (or less if the shock is collisionless). Behind the shock is a region of rapid radiative cooling. In the thick target case, this region is very thin. The shock and cooling region combined together form a "radiating shock", a structure well known in the astrophysics of supernova remnants, for example. If the condensation front is moving subsonically, then there is no radiating shock, but there is still a front present, which is approximately one radiative cooling length thick. For thick target heating, this cooling length is so short that the front remains quite thin.

In the thick target case, the radiating shock (if it exists) is followed by a region which is in quasi-steady energetic equilibrium, in which nonthermal electron heating balances radiative losses. This region makes up nearly all the mass of the condensation, with the radiating shock forming only at the very front. In fact, for the purposes of describing the jump in conditions on either side of the radiating shock (i.e. from in front of the condensation to within it) the radiating shock itself can be completely ignored: In the moving frame of the shock front, the conservation of ρv and $P + \rho v^2$ across the front as well as the constraint that thick target heating (per unit mass) must balance radiative losses on either side of the radiating shock, unambiguously specifies what the jump in hydrodynamic variables must be across the radiating shock. (This same argument holds true whether the "condensation front" consists of a radiating shock or not). If the plasma is completely ionized on both sides of the front (which for thick target heating is true), and if the dominant radiative losses are optically thin (which they are for thick target heating) specified by a power law ($\Lambda(T) = aT^{\alpha}$), the jump conditions across the condensation front are shown by FCMb to be:

$$(v_1/v_2) = (n_2/n_1) = (T_1/T_2)^{\alpha} = p^{1/\Gamma}, \tag{1}$$

$$M_1 = v_1/c_1 = \{[p-1]/[\Gamma(1 - p^{-1/\Gamma})]\}^{1/2}, \tag{2}$$

$$\dot{N} = n_1 v_1 = n_2 v_2 = n_1 c_1 M_1, \tag{3}$$

$$v_d = v_1 - v_2 = M_1 c_1 (1 - p^{-1/\Gamma}), \qquad (4)$$

where $p \equiv (p_2/p_1)$, $\Gamma \equiv (\alpha-1)/\alpha$, and $c_1 \equiv (\Gamma p_1/\rho_1)^{1/2}$ is the long wavelength limit of the sound speed in a plasma with optically thin losses balancing a heating rate constant per unit mass (Fisher, Canfield, and McClymont, 1985b, henceforth FCMb) Subscript 1 refers to material ahead of the condensation front, and 2 to the material behind the front (within the condensation itself). The application of these simple jump conditions to the thick target condensation shown in Fig. (1) describes its instantaneous evolution quite well.

The chromospheric condensation associated with the thermal model shows some significant differences from the thick target condensation. In the latter case, the conditions within most of the condensation are determined by quasi-steady energy balance, while the radiating shock forms only a thin layer at the front of the condensation. In the thermal model, there is no direct release of flare energy into the chromosphere. The unevaporated chromosphere remains much cooler overall, and hence has a much longer radiative cooling time. In this case, the cooling portion of the radiating shock encompasses virtually the entire condensation, i.e. there is essentially no region of quasi-steady energetic equilibrium. To complicate matters further, it is no longer true that the material on either side of the shock front is fully ionized. Ahead of the shock, the ionized fraction x is 10% or less, while immediately behind the shock the atmosphere is fully ionized during the initial condensation evolution. As the condensation weakens propagating into the chromosphere, the ionized fraction immediately behind the shock front begins to fall short of unity, and eventually the shock causes little change in the ionized fraction. Even early on, when the condensation is moving down rapidly, the ionized fraction drops from unity just behind the shock to roughly 0.15 at the back end of the condensation, adjacent to the flare transition region. The dominant radiative loss mechanism in the thermal model condensation varies according to position: Immediately behind the shock front, Balmer continuum recombination and losses from optically thick CaII and MgII dominate, while at the back end of the condensation, Lyman α and Lyman continuum losses dominate. The dominant loss mechanism for the thermal model condensation therefore cannot easily be specified in an optically thin manner.

In spite of the differences between condensations in the thick target and thermal model cases, and the various complexities associated with the thermal model condensation, there are a number of simple conclusions which can be drawn from the simulations:

(1) The downflow velocity of material within the condensation is independent of column depth although it is changing with time;

(2) In both thick target and thermal model cases, the condensations continually slow down as they propagate into the gravitationally stratified atmosphere. This is due to two effects. One of these is inertial, i.e. the density of the material ahead of the condensation increases with depth. The other effect is that the pressure jump across the condensation front, which actually drives the downflow, is decreasing as the pressure ahead of the condensation increases with

depth. A fairly good qualitative description of several of the flare simulations can be obtained by assuming that the pressure just behind the condensation front remains constant as the front propagates downward.

(3) In both heating models, the density within the condensation (n_2) is much greater than that ahead of it (n_1). This will remain true until the very last stages of the condensation's downward motion.

These observations allow one to develop a simple analytical model of condensation dynamics which reproduces the numerical results quite well. For example, using the preceding conclusions, it is straightforward to derive an 'equation of motion' for the condensation

$$\dot{N}^2 = (n_1/m)(P_2 - P_1) \tag{5}$$

where $\dot{N}$ is the column number accretion rate of the condensation front, n_1 and P_1 are the density and pressure of the material immediately ahead of the front, m is the mean mass per hydrogen nucleus, and P_2 is the pressure immediately behind the front, which is assumed for the moment not to vary with time. If the atmosphere ahead of the condensation is assumed to be in hydrostatic equilibrium (an excellent assumption for the thermal model, but somewhat questionable for the thick target model), described by a constant gravitational scale height H, then equation (5) can be integrated analytically. As a result, the time dependence of the condensation downflow velocity is found to be

$$v_d(t) = \pi(H/\tau)\ \cot\ [(\pi/2)(t/\tau + \alpha_0)], \tag{6}$$

where $\sin^2(\alpha_0) = N_0/N_{max}$, with $N_0/N_{max} << 1$ in general. N_0 is the initial formation depth of the condensation, N_{max} is the stopping depth ($N_{max} = P_2/mg$), and τ is the condensation lifetime

$$\tau = \pi(H/g)^{1/2}. \tag{7}$$

The actual downflow behavior for a thermal model simulation is described at least qualitatively by (6), as can be seen in Fig. (3), where the analytical result is compared to that from a simulation. The scale height H of 158 [km] is determined by an ionized fraction of 0.1 and a chromospheric temperature of 6660 [K], consistent with the mid chromosphere of our initial atmosphere, the Vernazza, Averett, and Loeser model F (1981).

The success of the above simple model in describing condensation dynamics allows the prediction of potentially observable quantities without knowing the detailed thermodynamic structure of the condensation itself. Suppose, for example, that the Hα red wing asymmetry often observed during flares is a measure of the condensation downflow speed $v_d(t)$, as has been proposed by Ichimoto and Kurokawa (1984). Then equation (6) predicts the temporal evolution of the velocity determined from the red wing asymmetry, and that the asymmetry should die away on a time scale of τ, which is about 1 minute for typical chromospheric values of the temperature and ionized fraction. It is interesting to note that this decay time is more or less independent of the impulsive phase heating mechanism assumed, although the magnitude of the initial

downflow speed seems in general to be greater for thick target heating. Even though time resolution of Hα asymmetries during flares is not sufficiently high to compare with the detailed temporal behavior of the simulations or with the analytical model, it is sufficiently good to show that the asymmetry decay time is roughly consistent with that predicted by (7). Studies are presently under way (Fisher, 1985) to develop more realistic analytical models of condensation dynamics which relax some of the assumptions used in deriving (6), but preliminary results show that the resulting decay times are fairly close to those given by (7), and that the initial evolution of the condensation is still described fairly well by (6). Observational studies are also underway to study the evolution of red wing asymmetries during flares with better time resolution (Canfield, 1985).

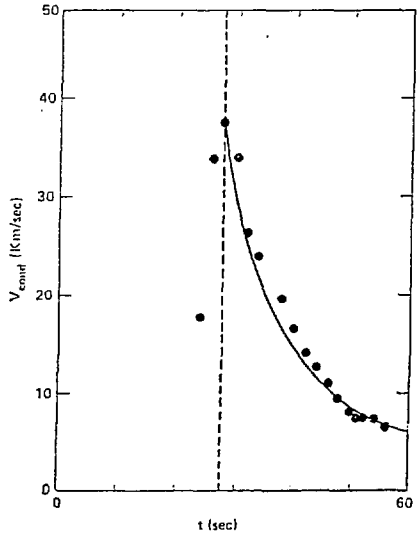

Figure 3. Comparison of condensation downflow speed computed in the thermal model simulation with the result (6). The dotted line corresponds to t=0 [s] in (6). The long delay before that corresponds to the motion of the conduction front through the corona

3. RADIATING SHOCKS.

In the preceding section the precise structure of the chromospheric condensation was glossed over, as such detailed knowledge is not necessary in order to understand the overall dynamics. However, the structure of the condensation, in particular the radiating shock which may form at its leading edge, can lead to distinct emission properties which could be used as a diagnostic of the temperature and density profiles in the radiating shock, in turn yielding information on energy deposition in the flaring atmosphere. The main observational

consequences of radiating shocks, if they form, is that they can provide a significant source of UV radiation in the impulsive phase of flares. In fact, as will be illustrated shortly, a radiating shock can produce much more of the emission normally associated with the transition region than does the transition region itself, at least during the transient period the radiating shock exists. To demonstrate this, the following section deals with the calculation of the differential emission measure ($\xi(T)$) in a radiating shock formed by thick target heating, and compares this with $\xi(T)$ from the transition region. In both cases, a simplified radiative loss rate is assumed.

The emission flux F from an optically thin, collisionally excited process in a plasma with a non-uniform distribution of temperature and electron density can often be expressed in the form

$$F = \int (g(T)/T)\xi(T)dT, \tag{8}$$

where $g(T)$ absorbs the details of the atomic physics of the given emission process, and $\xi(T)$ is the differential emission measure

$$\xi(T) = n_e^2 (d\ell nT/dz)^{-1}. \tag{9}$$

Because of this relationship between a measurable quantity (F), a supposedly known quantity ($g(T)$), and the model dependent quantity ($\xi(T)$), the differential emission measure can be an important contact point between theory and observation.

The structure of the transition region is often assumed to be determined by a balance between conductive heating and radiative losses, and as such yields the following behavior for $\xi(T_5) = \xi(T/10^5[K])$:

$$\xi_{tr}(T_5)\ [cm^{-5}] = 1.16 \times 10^{27}\ P\ T_5^{-3/4} \quad \text{for } T_5 < 1, \tag{10a}$$

$$\xi_{tr}(T_5)\ [cm^{-5}] = 1.16 \times 10^{27}\ P\ T_5^{3/2}[1 + 9(T_5^{1/2} - 1)]^{-1/2} \quad \text{for } T_5 > 1, \tag{10b}$$

where P is the transition region pressure [dyne cm^{-2}], and the optically thin radiative loss function is assumed to have the form

$$\Lambda(T_5)\ [erg\ cm^3\ s^{-1}] = 7 \times 10^{-22}\ T_5^3 \text{ for } T_5 < 1, \tag{11a}$$

$$\Lambda(T_5)\ [erg\ cm^3\ s^{-1}] = 7 \times 10^{-22}\ T_5^{-1} \text{ for } T_5 > 1, \tag{11b}$$

which has been demonstrated to be a reasonable approximation to the actual radiative losses during thick target heating (McClymont and Canfield 1983, FCMb). In fact, (10) is an upper limit to $\xi_{tr}(T)$, since the flare transition region is undergoing evaporation, a process which must reduce $\xi_{tr}(T)$ (Fisher, 1985).

In a radiating shock, it is straightforward to show by solving the steady state hydrodynamic equations in the shock reference frame that

$\xi(T)$ is approximately of the form

$$\xi_{rs}(T) = 5k\hat{N}\, T/\Lambda(T), \text{ for } T_{cond} < T < T_{max}, \qquad (12)$$

where T_{max} is determined by the strength of the shock and the temperature just ahead of it, and T_{cond} by the quasi-steady equilibrium condition in the bulk of the condensation. The quantity $\hat{N}$ is the instantaneous column number flux through the radiating shock. By applying values of $\hat{N}$ obtained from the simulations, one finds that $\xi_{rs}(T) >> \xi_{tr}(T)$ at a given instant in time for the allowed temperature range within the radiating shock. Therefore, emission from the radiating shock will dominate that from the transition region, and should therefore be observable. There are a number of further predictions one can make. As the condensation decelerates into the gravitationally stratified chromosphere, the shock strength will weaken, reducing the peak temperature achieved just behind the hydrodynamic shock. The emission from the highest temperatures in the radiating shock will therefore 'wink out' at some early point in time, with emission from successively lower temperatures disappearing at progressively later times. This behavior, if it in fact exists, should be clearly visible by an instrument such as the (recently crippled) Ultraviolet Spectrometer Polarimeter (UVSP) on board the Solar Maximum Mission.

In order to demonstrate this effect, and to show how the evolution of the radiating shock and condensation are tied together, one can combine the analytic behavior for the condensation downflow discussed in the previous section (to get an expression for $\hat{N}$) with the expression (12) for $\xi_{rs}(T)$. The condition that the atmosphere ahead of the radiating shock is in quasi-steady equilibrium between flare heating and radiative losses unambiguously determines the temperature just ahead of the radiating shock. Knowing also the condensation downflow speed unambiguously determines the Mach number, and hence the maximum temperature reached in the radiating shock at each point in time. It is therefore possible to predict the entire evolution of $\xi_{rs}(T)$ over the life of the radiating shock. (In the case illustrated in Fig. (4), it is 21 seconds. The subsequent condensation motion (lasting = 40 [s]) is subsonic). Three curves of $\xi(T)$ have been plotted in Fig. (4), corresponding to a specific case of thick target explosive evaporation. The dotted curve ($\xi_{rs}(T)$) is the differential emission measure from the radiating shock when it first forms. The dashed curve ($\xi_{tr}(T)$) is from the transition region at the same pressure as the condensation, and the solid curve ($\overline{\xi}_{rs}(T)$) is the <u>average</u> from the radiating shock over the length of time the radiating shock exists. One concludes that:

(1) At high time resolution, the radiating shock emission should be clearly visible over that from the transition region at all temperatures below the shock maximum, but

(2) At low time resolution $\xi_{tr}(T)$ dominates over $\overline{\xi}_{rs}(T)$ for temperatures above 10^5 [K]. Nevertheless, at low temperatures (below 10^5 [K]) $\overline{\xi}_{rs}(T)$ still dominates that from the transition region, and causes a much steeper temperature dependence of ξ: $\overline{\xi}_{rs}(T) \propto T^{-3.0}$. One concludes that UV instruments of rougnly 10 second time resolution should be able to detect emission from the lower temperature portion of

a radiating shock, and instruments with time resolution of 1 second or better should be able to detect the short lived emission from higher temperatures in radiating shocks.

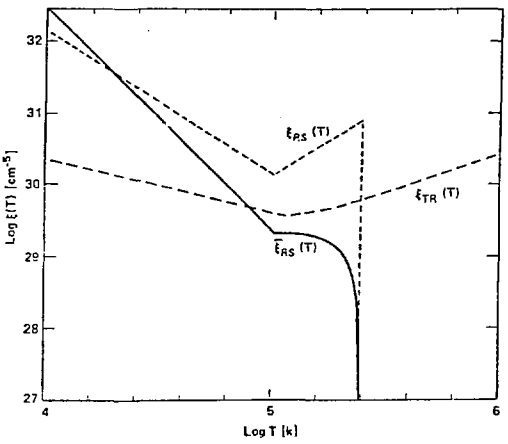

Figure 4. The dashed, dotted, and solid curves correspond to the differential emission measure from the transition region, the initial state of the radiating shock, and the average over the life of the radiating shock, respectively, for thick target heating similar to that used in Fig. 1

One significant piece of physics ignored in the entire preceding discussion is the question of ionization equilibrium. As is well known (Shull and McKee 1979, henceforth SM) the cooling time for an individual ion in a radiating shock can be shorter than its ionization equilibrium time scale, requiring a fully time dependent ionic species calculation to self-consistently determine the cooling rate in a radiating shock. Many such calculations have been done for radiating shocks in supernova remnants, for example SM, but at densities 11 or 12 orders of magnitude lower than the solar flare case. In the SNR case, important contributors to the loss rate include many forbidden and semi-forbidden transitions which would probably be quenched in the solar case. It is clear that calculations of the type performed by SM need to be done at much higher densities, and need to include the rapid weakening of the shock with time in order to make realistic predictions of specific UV spectral features. However, a study of non-equilibrium ionization effects in flares undertaken by MacNeice et al (1984) showed that the actual temperature structure in such a self-consistent calculation should not differ too much from that reflected by the ξ(T) calculations presented here using an ionization equilibrium radiative loss rate.

Radiating shocks in thermal model calculations seem to be significantly different from thick target radiating shocks. The chromospheric pressure enhancement due to evaporation by the conduction

front in general seems to be much less than that for explosive evaporation (Cheng et al 1983, Fisher, 1985). This results in a slower downflow speed, and hence a lower postshock temperature. In addition, the material ahead of the condensation is generally not ionized, as it has not been preheated by the nonthermal electrons. A great deal of the shock energy goes into simply ionizing the hydrogen, rather than heating the shocked material to high temperatures. As mentioned earlier, the characteristic emission in the thermal model radiating shock tends to be Balmer continuum recombination and optically thick CaII and MgII line radiation close to the shock front itself, and Lyman α and Lyman continuum radiation further toward the back (top) of the radiating shock. In contrast to the thick target case, there does not seem to be a large region of the thermal model condensation in quasisteady energetic equilibrium; the specific internal energy gradually decreases as the distance from the shock front increases. There is therefore no natural distinction between the radiating shock and the rest of the chromospheric condensation, as there is in the thick target case.

4. CONCLUSIONS

The motivation for performing detailed calculations of the radiative hydrodynamic response of loop models to flare energy release is that flare observations suggest that such models might have some realistic basis. As a result of performing these calculations, however, the situation has been turned around, and it is now possible to make new predictions of potentially observable phenomena based on these calculations. For example, if the thick target model of loop heating is to be taken at face value, then one expects that:

(1) Explosive evaporation at large electron energy fluxes will initiate a downward moving chromospheric condensation, producing observable red asymmetries in Hα, and the subsequent decay of these asymmetries on time scales of $\tau = \pi(H/g)^{1/2}$;

(2) Simultaneous with the initial downflow of a condensation, a bright radiating shock will form, emitting transition region-like UV radiation, but with the higher temperature emission rapidly 'winking out' as the shock decelerates. If it is possible to measure the downflow in the condensation sufficiently accurately, one should furthermore be able to link given downflow speeds with the disappearance of specific UV emission lines as the condensation slows down.

(3) The temperature dependence of the time averaged differential emission measure below 10^5 [K] should be overall somewhat steeper during flares than the quiet sun, where there presumably are no radiating shocks present.

I would like to thank Dr. Judy Karpen for carefully reading this paper.

REFERENCES:

An, C.H., Canfield, R.C., Fisher, G.H., McClymont, A.N.: Astrophysical Journal 267, 421. (1983)

Canfield, R.C.: Private communication. (1985)

Cheng, C.C., Oran, E.S., Doschek, G.A., Boris, J.P., Mariska, J.T.: Astrophysical Journal 265, 1090. (1983)

Fisher, G.H., Canfield, R.C., McClymont, A.N.: Astrophysical Journal 289, 414. (1985)

Fisher, G.H., Canfield, R.C., McClymont, A.N.: Astrophysical Journal 289, 434. (1985)

Fisher, G.H.: In prep. (1985)

Fisher, G.H.: In prep. (1985)

Ichimoto, K., Kurokawa, H.: Solar Physics 93, 105. (1984)

MacNeice, P., McWhirter, R.W.P., Spicer, D.S., Burgess, A.: Solar Physics 90, 357. (1984)

McClymont, A.N., Canfield, R.C.: Astrophysical Journal 265, 497. (1983)

Shull, J.M., McKee, C.F.: Astrophysical Journal 227, 131 (1979)

Vernazza, J.E., Averett, E.H., Loeser, R.: Astrophysical Journal (Supplement) 45, 619. (1981)